HHS Public Access

Author manuscript

*Nat Med*. Author manuscript; available in PMC 2015 June 01.

Published in final edited form as:

*Nat Med*. 2014 December ; 20(12): 1444–1451. doi:10.1038/nm.3717.

# Alterations in microRNA-124 and AMPA receptors contribute to social behavioral deficits in frontotemporal dementia

**Eduardo Gascon**[1], **Kelleen Lynch**[1], **Hongyu Ruan**[2], **Sandra Almeida**[1], **Jamie Verheyden**[3,#], **William W. Seeley**[4], **Dennis W. Dickson**[5], **Leonard Petrucelli**[5], **Danqiong Sun**[3,&], **Jian Jiao**[3,§], **Hongru Zhou**[1], **Mira Jakovcevski**[6], **Schahram Akbarian**[6,†], **Wei-Dong Yao**[2,f], and **Fen-Biao Gao**[1,*]

[1]Department of Neurology, University of Massachusetts Medical School, Worcester, MA, 01605 USA

[2]Division of Neurosciences, New England Primate Research Center, Harvard Medical School, Southborough, MA, 01772 USA

[3]Gladstone Institute of Neurological Disease, San Francisco, CA 94158 USA

[4]Memory and Aging Center, Department of Neurology, University of California, San Francisco, CA 94143, USA

[5]Department of Neuroscience, Mayo Clinic Florida, Jacksonville, FL 32224, USA

[6]Brudnick Neuropsychiatric Research Institute, Department of Psychiatry, University of Massachusetts Medical School, Worcester, MA 01604, USA

## Abstract

Many neurodegenerative diseases, such as frontotemporal dementia (FTD), are associated with behavioral deficits, but the anatomical and molecular bases remain poorly understood. Here we show that forebrain-specific expression of FTD-associated mutant CHMP2B causes several age-dependent neurodegenerative phenotypes, including social behavioral impairments. The social deficits were accompanied by a change in AMPA receptor (AMPAR) composition, leading to imbalance between $Ca^{2+}$-permeable and -impermeable AMPARs. Expression of most AMPAR



*Correspondence to Fen-Biao Gao, Department of Neurology, University of Massachusetts Medical School, Worcester, MA 01605; fen-biao.gao@umassmed.edu.

#Present address: Laboratory of Genetics, University of Wisconsin-Madison, Madison, WI 53706, USA.

&Present address: System Biosciences, 265 N. Whisman Road, Mountain View, CA 94043.

§Present address: NGM Biopharmaceuticals, 630 Gateway Blvd., South San Francisco, CA 94080, USA.

†Present address: Departments of Psychiatry and Neuroscience, Friedman Brain Institute, Icahn School of Medicine at Mount Sinai, New York, NY 10029 USA.

fPresent address: Departments of Psychiatry and Neuroscience, SUNY Upstate Medical University, Syracuse, NY 13210 USA.

**Accession Numbers**. Microarray and deep sequencing data[39,40] are available at the NCBI Gene Expression Omnibus database under series accession numbers GDS3459 and GPL10999.

**AUTHOR CONTRIBUTIONS**

EG, KL, SA, and HZ performed most experiments. HR and WDY carried out the electrophysiology analysis and wrote the relevant sections. JV, DS, and JJ generated the transgenic mouse lines. LP, DWD, and WWS provided brain tissues from controls and subjects with FTD. MJ and SA assisted with behavioral tests. EG and FBG analyzed the data and wrote the manuscript. FBG conceived and supervised the project.

subunits was regulated by the brain-enriched microRNA (miR-124), whose abundance was markedly decreased in the superficial layers of cerebral cortex of FTD mice. We found similar changes in miR-124 and AMPAR levels in the frontal cortex and iPSC-derived neurons of subjects with behavioral variant FTD. Moreover, miR-124 expression in the medial prefrontal cortex decreased AMPAR levels and partially rescued behavioral deficits. Knockdown of *Gria2* also alleviated social impairments in FTD mice. Our results identify a novel mechanism involving miR-124 and AMAPRs in regulating social behavior in FTD and suggest a potential therapeutic avenue.

**Keywords**

AMPA receptor; CHMP2B; frontotemporal dementia; microRNA; neurodegeneration; social behavior

---

Different neurodegenerative diseases are characterized by progressive dysfunction and loss of specific neuronal populations, often resulting in various behavioral abnormalities[1-3]. The molecular mechanisms of these impairments, and the neural circuits involved, are poorly understood. Frontotemporal dementia (FTD) is the second most common cause of dementia before 65 years of age. More than 50% of subjects with FTD have the behavioral variant, characterized by marked changes in personality and social behavior[4]. FTD has a strong genetic component; about 40% of subjects have a family history of the disease[5]. FTD is linked clinically, pathologically, and molecularly to amyotrophic lateral sclerosis[6,7].

Mutations in several seemingly unrelated genes cause familial FTD[6,7]. However, the clinical outcome in subjects with FTD carrying different mutations is often similar, suggesting that the same neural circuits are affected. Mutations in *charged multivesicular body protein 2B* (*CHMP2B)* are especially interesting, as they are implicated not only in FTD and amyotrophic lateral sclerosis[8,9] but also recently in early-onset Alzheimer's disease[10]. *CHMP2B* encodes a component of the endosomal sorting complexes required for transport-III (ESCRT-III), which functions in the endosomal-lysosomal and autophagy pathways[11,12]. The mutation that causes FTD results in a C-terminally truncated CHMP2B ($CHMP2B^{Intron5}$)[9] and a number of studies suggest a gain-of toxic function unique to the $CHMP2B^{Intron5}$ isoform[13-16].

Although the molecular basis of the social deficits associated with FTD is unknown, microRNAs (miRNAs), a class of small noncoding RNAs, are important contributors to neurodegeneration[17,18]. In that regard, miR-124 is an attractive candidate because it is evolutionary conserved and one of the most abundant miRNAs in the brain. Although miR-124 has well-established functions during neuronal development[19], its specific roles in neurodegeneration are poorly understood[17,18]. Here, through a novel mouse model of FTD with the $CHMP2B^{Intron5}$ mutation and studies on iPSC-derived human neurons and brain tissues of behavioral variant FTD (bvFTD), we uncovered unexpected contributions of miR-124 and AMPA receptors (AMPARs) to FTD-associated social impairments.

# RESULTS

## A novel mouse model of FTD exhibits deficits in sociability

To examine the molecular basis of behavioral abnormalities in FTD, we generated a novel transgenic mouse model expressing, under the control of the tetracycline promoter, CHMP2B$^{Intron5}$ (Fig. 1a). When crossed with a reporter line (*TetO-GFP*), *CamkII*a-*tTA* drives GFP expression starting around E18 in forebrain neurons (Supplementary Fig. 1a). We then crossed *CaMKII*a-*tTA* mice with different *CHMP2B*$^{WT}$ or *CHMP2B*$^{Intron5}$ founder lines. Transgene expression pattern in *tTA:CHMP2B*$^{WT}$ and *tTA:CHMP2B*$^{Intron5}$ mice was very similar to that of the reporter GFP (Supplementary Fig. 1b).

The extent of transgene expression was modest at both the mRNA level (Supplementary Fig. 1c) and the protein level (Supplementary Fig. 1e) in *tTA:CHMP2B*$^{WT}$ and *tTA:CHMP2B*$^{Intron5}$ mice. We selected *tTA:CHMP2B*$^{WT}$ line 3 and *tTA:CHMP2B*$^{Intron5}$ line 3 for further analysis in most experiments because of their equal transgene expression at the mRNA level (Supplementary Fig. 1c) and because CHMP2B$^{Intron5}$ and CHMP2B$^{WT}$ proteins are equally stable[15]. Moreover, a doxycycline-containing diet repressed transgene transcription (Supplementary Fig. 1d).

To determine whether our mice have disease-relevant behavioral deficits, we first used the resident-intruder test[20]. Although *tTA:CHMP2B*$^{Intron5}$ mice performed similarly to *tTA:CHMP2B*$^{WT}$ mice at the beginning of the test, their interaction times at the last two time points decreased (Supplementary Fig. 2a), suggesting specific defects in this social behavior. To further characterize the social behavioral deficits, we used a modified version of the three-chamber social paradigm[21]. In Trial 2, both *tTA:CHMP2B*$^{WT}$ and *tTA:CHMP2B*$^{Intron5}$ mice spent equally more time in the target chamber that contains Stranger 1 than in the empty chamber (Fig. 1b), indicating that *CHMP2B*$^{Intron5}$ expression does not perturb the ability to recognize a conspecific mouse.

To quantify sociability, we measured the time test mice spent in close interaction with social partners across trials. In Trial 2, both *tTA:CHMP2B*$^{WT}$ and *tTA:CHMP2B*$^{Intron5}$ mice showed equal sociability, which gradually decreased in later trials, suggesting progressive loss of social interest in the familiar mouse (Fig. 1c). However, *tTA:CHMP2B*$^{Intron5}$ mice had a more pronounced, age-dependent decrease in sociability, particularly in Trial 5, when both social partners were present (Fig. 1c). We also observed a similar age-dependence in the elevated plus maze (Supplementary Fig. 2c). In Trial 5, the proportion of time *tTA:CHMP2B*$^{Intron5}$ mice spent interacting with Stanger 2 was similar to that of *tTA:CHMP2B*$^{WT}$ mice, suggesting that they distinguished Stranger 1 from Stranger 2 equally well (Fig. 1d). Moreover, time spent in each chamber during Trial 5 did not differ between *tTA:CHMP2B*$^{Intron5}$ and *tTA:CHMP2B*$^{WT}$ mice (Fig. 1e), suggesting that social behavior but not exploration pattern is specifically compromised in mutant mice. Moreover, in a novel object recognition task in which exploration can be assessed independently of social cues, the times exploring identical objects during the familiarization phase as well as the familiar and novel object during the test phase were similar in *tTA:CHMP2B*$^{Intron5}$ and *tTA:CHMP2B*$^{WT}$ mice (Supplementary Fig. 2d), confirming the specificity of the social deficits.

The selective effect of CHMP2B$^{Intron5}$ is also supported by the lack of major deficiency in locomotion (Supplementary Fig. 2e). Moreover, it is unlikely that the social deficits were due to perturbed olfaction, as we did not observe gross morphological defects in the olfactory bulb (Supplementary Fig. 3a,b). Moreover, *tTA:CHMP2B$^{Intron5}$* showed no differences from *tTA:CHMP2B$^{WT}$* mice at 8 months of age in the time spent with either two supposedly preferred scents (cinnamon and vanilla) or an aversive scent (2-methyl butyrate) (Supplementary Fig. 2f), suggesting that their olfactory discrimination is not disrupted.

Thus, the FTD mice have a selective impairment in sociability. Moreover, seven of 36 old *tTA:CHMP2B$^{Intron5}$* mice (age 14-20 months) had cutaneous lesions compatible with excessive grooming, suggesting an obsessive-compulsive-like behavior (Supplementary Fig. 2b). Together, these results indicate that expression of CHMP2B$^{Intron5}$ in the mouse forebrain causes age-dependent behavioral deficits that recapitulate some of the clinical symptoms of bvFTD.

## AMPAR composition is altered in the cortex of tTA:CHMP2B$^{Intron5}$ mice

To investigate the cellular and molecular bases of the behavioral deficits, we found that at 8 months of age, forebrain structures of *tTA:CHMP2B$^{Intron5}$* mice were similar to those of *tTA:CHMP2B$^{WT}$* mice (Supplementary Fig. 3a,b) and showed no obvious neuronal loss (Supplementary Fig. 3c,d). However, *tTA:CHMP2B$^{Inton5}$* mice had some FTD-like histopathological features, including astrogliosis, ubiquitin deposits, and an increase of p62 in insoluble fraction (Supplementary Fig. 4a-d). In addition, in pyramidal neurons in the superficial layers (II and III) of the medial prefrontal cortex (mPFC)—which are most vulnerable in subjects with FTD[22,23]—spine number and density were greater in *tTA:CHMP2B$^{Inton5}$* than in *tTA:CHMP2B$^{WT}$* mice (Supplementary Fig. 3e,f). This increase was largely due to “thin” spines, which are considered immature[24-26]. We did not observe spine changes in hippocampal CA3 pyramidal neurons (Supplementary Fig. 3f), consistent with a greater susceptibility of certain neuronal populations in the mPFC.

To further examine synaptic defects, we first analyzed glutamate receptor levels and composition. qRT-PCR analysis of the various NMDA and kainate subunits showed no apparent differences between *tTA:CHMP2B$^{Intron5}$* and *tTA:CHMP2B$^{WT}$*mice (Fig. 2a). However, in *tTA:CHMP2B$^{Intron5}$* mice, mRNAs encoding AMPAR subunits Gria2, Gria3, and Gria4 but not Gria1 were upregulated at 4 and 8 months of age (Fig. 2a), correlating with the age-dependent defects in sociability. Then we analyzed postsynaptic density (PSD) fractions from the cortex of *tTA:CHMP2B$^{Intron5}$* and *tTA:CHMP2B$^{WT}$* mice. Interestingly, NMDA subunits and Gria1 were maintained at similar levels in *tTA:CHMP2B$^{Intron5}$* mice at all time points examined, whereas Gria2, Gria3, and Gria4 levels were increased substantially in mice aged 4 months and older (Fig. 2b and Supplementary Fig. 5a). Moreover, *tTA:CHMP2B$^{Intron5}$* mice at 8 months of age had a higher number of Gria2$^{+}$PSD95$^{+}$ (Fig. 2c) and Gria4$^{+}$PSD95$^{+}$ (Supplementary Fig. 5b) puncta in the mPFC, confirming the increased synaptic content of these subunits *in situ*. Thus, an age-dependent dysregulation of AMPAR subunit composition correlates with the onset of behavioral deficits in *tTA:CHMP2B$^{Intron5}$* mice.

## AMPAR function in the mPFC is altered in tTA:CHMP2B$^{Intron5}$ mice

We next sought to link altered postsynaptic AMPARs to social defects in *tTA:CHMP2B*$^{Intron5}$ mice. In 8-month old *tTA:CHMP2B*$^{WT}$ mice, intraperitoneal injection of NBQX (50 mg kg$^{-1}$), a general AMPAR antagonist[27], did not modify sociability (Fig. 3a). In 8-month-old *tTA:CHMP2B*$^{Intron5}$ mice, however, NBQX increased sociability, suggesting that an abnormal AMPAR activity might underlie the social defects in these mice (Fig. 3a). Injections of saline or the NMDA receptor antagonist AP5 (10 mg kg$^{-1}$) did not affect sociability (data not shown) in either *tTA:CHMP2B*$^{Intron5}$ or *tTA:CHMP2B*$^{WT}$ mice. Thus, these results, together with the changes in AMPAR composition in the cortex of *tTA:CHMP2B*$^{Intron5}$ mice (Fig. 2), suggest that impaired social behaviors result from postsynaptic perturbation of synaptic AMPARs.

To further investigate AMPAR alterations at the functional level in FTD mice, we examined the electrophysiological properties of synapses in layers II and III made on apical dendrites of layer V pyramidal neurons in the mPFC in acute brain slices from 15-16-week-old mice. The amplitude or frequency of AMPAR-mediated miniature excitatory postsynaptic currents (AMPAR-mEPSCs) was not altered in *tTA:CHMP2B*$^{Intron5}$ mice (Fig. 3b), suggesting that the presynaptic release mechanism or the overall synaptic strength of these neurons at the resting level was largely intact in the mutant mice.

Most AMPARs in principal excitatory neurons contain Gria2 and hence are $Ca^{2+}$-impermeable[28]. However, some AMPARs lack Gria2[29], causing these receptors to be $Ca^{2+}$-permeable and exhibit an inwardly rectifying current-voltage relationship due to voltage-dependent blockade by intracellular polyamines[30,31]. Since Gria2 expression was increased in *tTA:CHMP2B*$^{Intron5}$ mice (Fig. 2), one would expect a functional increase in the proportion of Gria2-containing AMPARs in mutant synapses. To test this hypothesis, we recorded AMPAR-mediated EPSCs in response to stimuli delivered to layer II and III at −60 and +60 mV and calculated the rectification index, $EPSC_{-60mV}/EPSC_{+60mV}$. Synapses of *tTA:CHMP2B*$^{Intron5}$ mice had a lower rectification index than those of *tTA:CHMP2B*$^{WT}$ mice (Fig. 3c), suggesting an increased proportion of Gria2-containing receptors. Moreover, at a concentration of 200 μM, Naspm (a specific inhibitor of $Ca^{2+}$-permeable AMPARs)[32] partially blocked AMPAR-mediated currents in *tTA:CHMP2B*$^{WT}$ neurons, indicating the existence of a substantial amount of AMPARs lacking Gria2 under control conditions. In contrast, EPSCs of *tTA:CHMP2B*$^{Intron5}$ neurons were less sensitive to inhibition by Naspm (Fig. 3d), again indicating an altered AMPAR subunit composition characterized by an enrichment of Gria2-containing $Ca^{2+}$-impermeable receptors. Thus, our data suggest that Gria2-lacking AMPARs exist in mPFC neurons of adult *tTA:CHMP2B*$^{WT}$ mice and that these native $Ca^{2+}$-permeable receptors are replaced by Gria2-containing, $Ca^{2+}$-impermeable AMPARs in *tTA:CHMP2B*$^{Intron5}$ mice.

## MiR-124 regulates AMPAR levels and is decreased in the cortex of *t*TA:CHMP2B$^{Intron5}$ mice

We next examined mechanisms of the upregulation of AMPARs in *tTA:CHMP2B*$^{Intron5}$ mice. We turned our attention to miRNAs, as they control gene expression at the posttranscriptional level[33] and are essential regulators of synaptic function[34]. Furthermore, each miRNA can regulate multiple mRNA targets that may contribute to complex processes,

such as sociability. We examined the expression levels of a number of brain-enriched miRNAs in the cortex in *tTA:CHMP2B*$^{Intron5}$ mice at one month and at one year of age. At both time points, many miRNAs were expressed in the cortex at similar levels in *tTA:CHMP2B*$^{Intron5}$ mice and *tTA:CHMP2B*$^{WT}$ mice (Supplementary Fig. 6b); however, at one year, some miRNAs were downregulated in *tTA:CHMP2B*$^{Intron5}$ mice, especially miR-124, which is one of the most abundant miRNAs in the brain (Supplementary Fig. 6a,b). miR-124 downregulation was specific to the expression of the FTD-causing CHMP2B$^{Intron5}$, as these miRNAs remained unchanged in the cerebellum, where the transgene was not expressed (Supplementary Fig. 6a). Importantly, miR-124 was also downregulated to a lesser extent in the cortex of two other independent transgenic lines expressing lower level of *CHMP2B*$^{Intron5}$ (Supplementary Fig. 6c). In contrast, variable levels of *CHMP2B*$^{WT}$ expression in the other mouse lines did not affect miR-124 abundance (Supplementary Fig. 6c). Moreover, when CHMP2B$^{Intron5}$ expression was turned off in *tTA:CHMP2B*$^{Intron5}$ mice fed a diet containing doxycycline (Supplementary Fig. 1d), their cortical miR-124 expression was identical to that in *tTA:CHMP2B*$^{WT}$ mice fed a regular diet or a diet containing doxycycline (Supplementary Fig. 7a). These results support a specific correlation between *CHMP2B*$^{Intron5}$ expression and miR-124 reduction.

Computer algorithms (Targetscan, PicTar, miRanda) indicate that three AMPAR subunits, Gria2, Gria3, and Gria4, are potential targets of miR-124 (Fig. 4a). Thus, downregulation of miR-124 might contribute to the upregulation of these AMPARs in *tTA:CHMP2B*$^{Intron5}$ mice. Indeed, in transfected HEK293 cells, miR-124 markedly suppressed the expression of the reporter gene with the 3′UTRs of Gria2, Gria3, and Gria4 but not of Gria1 (Fig. 4b). Their expression was not suppressed when we mutated the miR-124 binding site (Fig. 4c). Similarly, in the cortex of *tTA:CHMP2B*$^{Intron5}$ mice, miR-9 levels remained unchanged, whereas miR-124 was downregulated in an age-dependent manner (Fig. 4d,e), correlating with the age-dependent increase in Gria2, Gria3, and Gria4 levels (Fig. 2) and the social behavioral deficits (Fig. 1).

Consistent with previous studies[35], miR-124 was widely expressed in all layers of the cortex of 2-month-old mice (Supplementary Fig. 7b). In contrast, miR-124 expression was markedly decreased in the cortex of *tTA:CHMP2B*$^{Intron5}$ mice at 8 months of age, and this decrease seemed to be most pronounced in the layers II and III (Fig. 4f). Most neurons expressing miR-124 at low levels in the superficial layers were also strongly positive for CHMP2B$^{Intron5}$ (Fig. 4g,h). Thus, expression of CHMP2B$^{Intron5}$ triggers a progressive loss of miR-124 that is greater in superficial layers.

## miR-124 and AMPARs are dysregulated in a subset of subjects with behavioral variant FTD

To confirm that our findings in mice are relevant to human disease, we next examined miR-124 and AMPAR levels in subjects with FTD. Since FTD is a heterogeneous disorder, we focused on the frontal cortex, a brain region critical for social behavior, in a subset of subjects with the behavioral variant (bvFTD), whose clinical presentation is closest to the phenotypes in our mice. In samples from two brain banks, we found a decrease in miR-124, but not miR-9, and a concomitant upregulation of *GRIA2* and *GRIA4* in the frontal cortex of five bvFTD cases compared with five age-matched controls (Fig. 5a).

Then we took advantage of induced pluripotent stem cell lines derived from three subjects with bvFTD we established previously[36,37]. The levels of miR-124 and AMPARs in 2-week-old neurons derived from four iPSC lines of three subjects with bvFTD were the same as those in controls (Fig. 5b). However, in 8-week old neurons of subjects with bvFTD, miR-124 was substantially reduced and some AMPAR subunit mRNAs were upregulated (Fig. 5c). This change is not due to culture condition since the percentages of different neuronal subtypes remained the same as those in cultures derived from controls (Supplementary Fig. 8a). As controls, the miR-9 level was not decreased (Fig. 5c) and we did not detect a change in NMDA or kainate receptor transcripts or neuronal subtype-specific markers (Supplementary Fig. 8a,b).

To further confirm this finding, we surveyed published genome-wide studies of miRNAs on frontal cortex samples from subjects with FTD[38]. Re-analysis of the data showed a decrease in miR-124 level in the frontal cortex of subjects with progranulin deficiency (FTD-GRN) (Supplementary Fig. 9a). Another published study, of a small number of subjects, also showed a trend toward a decrease[39]. Similarly, re-analysis of a published transcriptome profiling data[40] revealed an increase in some AMPAR subunits, but not of some NMDA receptor subunits, in the frontal cortex but not the cerebellum of six subjects with FTD-GRN (Supplementary Fig. 9b,c). These data are relevant to our study since most subjects with FTD-GRN belong to the behavioral variant[41]. Together, these findings suggest that dysregulation of miR-124 and AMPARs discovered in our mouse model also occurs in the frontal cortex in a subset of subjects with bvFTD.

## MiR-124 expression and Gria2 knockdown in the mPFC partially rescue social deficits in *t*TA:CHMP2B$^{Intron5}$ mice

To determine whether miR-124 downregulation contributes to FTD-associated social deficits in *tTA:CHMP2B*$^{Intron5}$ mice, we engineered an adeno-associated vector (AAV) to express miR-124 *in vitro* (Supplementary Fig. 10a) and *in vivo* (Fig. 6a). The mPFC controls most social behaviors in mice[42], and we detected synaptic defects in that region in *tTA:CHMP2B*$^{Intron5}$ mice (Fig. 2). Therefore, we injected an AAV driving miR-124 expression or a control AAV-GFP vector into the mPFC of 7-month-old mice.

We first observed that AAV-mediated miR-124 expression reduced mRNA levels of *Gria2* and *Gria4* in the mPFC of *tTA:CHMP2B*$^{Intron5}$ mice (Fig. 6b). The decrease was not due to the surgical procedure, since mRNA levels did not differ in the occipital cortex of the same mice (Supplementary Fig. 10b). Although we could not obtain enough material from these experiments for PSD fractionation, we did find a decrease in the number and the intensity of synaptic Gria2 puncta in brain sections (Fig. 6c). More importantly, AAV-GFP injection did not improve the sociability of *tTA:CHMP2B*$^{Intron5}$ mice at either 1 or 2 months (Fig. 6d). In contrast, one month after injection of AAV-GFP-miR-124, the mice showed a substantial increase in sociability in Trial 5. These mice showed a further improvement at 2 months that was significantly better than the pre-injection level ($P < 0.001$), suggesting that the deficits were reversed (Fig. 6d). Finally, the time spent with Stranger 2 did not differ in AAV-GFP mice and those injected with AAV-GFP-miR-124 (Supplementary Fig. 10c), arguing for a role of miR-124 in specifically regulating sociability but not novelty recognition.

To further demonstrate that a decrease in $Ca^{2+}$-impermeable AMPARs contributes to the social deficits in *tTA:CHMP2B*$^{Intron5}$ mice, we constructed lentiviral vectors expressing scrambled short-hairpin RNA (shRNA) or shRNA directed against mouse *Gria2* (Supplementary Fig. 11a). After lentivirus injection into the mPFC of 7-month-old *tTA:CHMP2B*$^{Intron5}$ mice, downregulation of *Gria2* expression partially rescued the social deficits (Fig. 6e). Interestingly, recognition of the novel mouse (Stranger 2) during this trial was not affected (Supplementary Fig. 11b), suggesting that Gria2 levels are critical for sociability but not all aspects of social behavior. Together, these results support the notion that alterations in AMPARs composition in the mPFC contribute to social defects in *tTA:CHMP2B*$^{Intron5}$ mice.

## DISCUSSION

In a novel mouse model of FTD harboring the CHMP2B$^{Intron5}$ mutation, we found that downregulation of miR-124 causes a dysregulation in AMPAR composition and a selective impairment in sociability. AAV-mediated ectopic expression of miR-124 in the mPFC partially restored the levels of AMPAR subunits and rescued the social behavioral deficits. Knockdown of Gria2 also alleviated the social deficits in FTD mice, suggesting a key role for $Ca^{2+}$-impermeable AMPARs. Similar alterations in miR-124 and AMPAR levels were also found in human cortical neurons derived from iPSCs of subjects with bvFTD and in the frontal cortex of a subset of subjects with bvFTD. Thus, the mechanisms uncovered in our mouse model of FTD may have general implications for understanding behavioral abnormalities in human subjects with the disease.

Marked changes in social behavior such as social withdrawal and obsessive-compulsive behaviors are common in subjects with bvFTD[4,43]. Social deficits similar to those in our *tTA:CHMP2B*$^{Intron5}$ mice were also reported in progranulin haploinsufficient mice[44], an independent FTD model. In addition, a number of FTD histopathological hallmarks were present in our mice and previously published mouse models[14,44], suggesting that the anatomical and behavioral abnormalities in subjects with FTD can be reproduced in mice. Despite widespread forebrain expression of mutant CHMP2B$^{Intron5}$ protein in our FTD mice, only sociability was impaired at an early age, indicating that specific circuits are particularly vulnerable. Consistent with this notion, neurons in some regions of the human prefrontal cortex are most susceptible in FTD[45]. Moreover, ectopic miR-124 expression or Gria2 knockdown in this cortical area partially rescued the social behavioral deficits.

Our findings suggest that AMPAR composition is regulated by miR-124 and altered in FTD mice. More importantly, we also found miR-124 downregulation and a concomitant increase in AMPARs levels in the frontal cortex and iPSC-derived cortical neurons from subjects with bvFTD. AMPARs have been implicated in social behaviors. For instance, *Gria3* knockout mice show increased aggression[46]. Modulating AMPAR activity in the mPFC can result in both upward and downward movement in the social hierarchy[42]. Our electrophysiological analysis suggested that FTD-related social behaviors are linked to an increase in $Ca^{2+}$-impermeable AMPARs at excitatory synapses of PFC pyramidal neurons. These abnormally inserted receptors may interfere with synaptic $Ca^{2+}$ signaling or impair synaptic efficacy and plasticity[47], leading to structural alterations in dendritic spines and

behavioral deficits in social interaction. We speculate these molecular changes may also contribute to the early behavioral abnormalities in subjects with FTD as well.

MiRNAs are deregulated in many neurodegenerative disorders[18]. The exact molecular link between CHMP2B$^{Intron5}$ mutation and miR-124 reduction remains to be elucidated. However, previous works implicated a role of ESCRTs in the miRNA pathway[48,49], raising the possibility that CHMP2B$^{Intron5}$ mutation could affect miR-124 stability. Only six of 91 neurotransmitter receptor subunit mRNAs are predicted targets of miR-124, including three of four known AMPAR subunits (Supplementary Table 1). Thus, miR-124 may play a unique role in fine-tuning glutamate neurotransmission by controlling the expression and composition of AMPARs, consistent with the inverse correlation between miR-124 and Gria2 levels reported here and by others[50]. Moreover, our finding that ectopic expression of miR-124 or Gria2 knockdown partially rescues behavioral deficits in early stages of FTD may suggest a potentially beneficial therapeutic approach before neuronal cell loss becomes apparent and irreversible.

## ONLINE METHODS

### Mice

All procedures involving mice were approved by the University of Massachusetts Medical School Institutional Animal Care and Use Committee. We cloned *CHMP2B$^{WT}$* and *CHMP2B$^{Intron5}$* into the NotI and SalI sites of pTRE-Tight-BI-ZsGreen1 mammalian expression vector (Clontech). We linearized pTRE-*CHMP2B$^{WT}$* vector with BsrBI, and purified DNA for microinjection. Since no adequate restriction enzymes were present on the pTRE-*CHMP2B$^{Intron5}$* plasmid, we amplified the cassette by PCR (TRESacIIFwd 5′-CCGCGGCCACCTGACGTCG GCAGT GAA-3′ and TREApaIRV 5′-GGGCCCCGAGTCAGTGAGCGAGGAAGCTC-3′) and subcloned into pCR2.1 TOPO (Invitrogen). We linearized this construct with SacII and ApaI enzymes, and purified DNA for microinjection. For both CHMP2B$^{WT}$ and CHMP2B$^{Intron5}$ constructs, ZsGreen coding sequence was lost after linearization. Injected eggs were transferred to female recipients, and F1 litters analyzed for transgene insertion by PCR with two specific sets of primers (forward primer: 5′-GCTCGTTTAGTGAACCGTCAG-3′; reverse primer: 5′-AGCTC GGGGCAGTGAAAA-3′ or forward primer 5′-ATGGCGTCCCTCTTCAAGAAGA AAAG-3′ and reverse primer 5′-GGGCCCCGAGTCAGTGAGCGAGGAAGCTC-3′).

We maintained germline-transmitting founders (three for *CHMP2B$^{WT}$* and three for *CHMP2B$^{Intron5}$*) as hemizygous lines by backcrossing to wildtype C57BL/6 mice. To drive transgene expression in the forebrain, we crossed *CHMP2B$^{WT}$* and *CHMP2B$^{Intron5}$* transgenic mice with *CaMKII*α-*tTA* mice (Jackson Laboratory 003010**)**. We used both male and female double-transgenic offspring for all experiments.

### Behavioral tests

We conducted all experiments between 9 am and 5 pm. We housed mice under specific-pathogen-free conditions in an animal facility with a regular 12-h light and dark cycle (light

on at 7:00 am) under constant conditions (21 ± 1 °C; 60% humidity). Food and water were supplied ad libitum.

We conducted all behavioral studies using both male and female mice and analyzed data blind to genotypes. For all tasks, each mouse was selected randomly and then tested on the same day. We tested the first cohort of mice for sociability in the three-chamber social approach task. 2 d after the social test, we tested subjects in the open field and, 2 d later, in the elevated plus maze. We used independent cohorts of mice at 8 months of age for the other tests; these mice were not subjected to any other task.

### Open field

We tested general exploratory locomotion in a novel open-field environment in 15 min sessions in a 40 × 40 × 40 cm white Plexiglas arena. The mouse was placed in the center of the arena and allowed to freely move while being recorded by an overhead camera. We analyzed behavior with an automated tracking system (Ethovision software, Noldus). The total distance traversed in the arena and the time spent in the center vs. the perimeter were automatically calculated.

### Elevated plus maze

The elevated plus maze (Med Associates) consisted of two open arms and two closed arms situated opposite each other and separated by a 6 cm square center platform. Each runway is 6 cm wide × 35 cm long. The open arms have lips 0.5 cm high to prevent mice from slipping off the arm, and the closed arms are surrounded on three sides by 20 cm high walls. The floors and walls are black polypropylene. For each test, the mouse was placed in the center square facing the open arms and allowed to explore freely for 5 min. The number of entries in the open and closed arms and the times spent in the open arms, closed arms, and the center square were quantified by automated analysis of beam breaks.

### Three-chamber social task

We evaluated sociability, social recognition, and response to social novelty by using the three-chamber task with minor modifications. Test mice were housed individually for 1 week before the test. We habituated the mice in the testing room for at least 1 min before the start of behavioral tasks. The social test apparatus consisted of a white Plexiglas box with removable floor and partitions dividing the box into three chambers with 5 cm openings between chambers. Target subjects (Stranger 1 and Stranger 2) were 10-14 week old males. We used wire cages to contain the stranger mice. We placed a paper cup on the top of the cage to prevent the test mice from climbing on the top of the wire cage. This task was carried out in five trials of 5 min each. After each trial, we returned the mouse to his home cage for 15 min.

- Trial 1: the test mouse is placed to the middle chamber and left to explore the arena containing the empty wire cages for 5 min (habituation).
- Trials 2–4: the mouse is placed in the middle chamber, but an unfamiliar mouse (Stranger 1) is placed into a wire cage in one of the side-chambers (the wire cage in the other side-chamber remains empty) (sociability, social learning acquisition).

- Trial 5: a novel stranger mouse (Stranger 2) is placed in the previously empty wire cage and again the test mouse is left to explore for 5 min (sociability, social recognition memory).

We recorded and analyzed all the trials *post hoc*. We measured the time spent in each chamber and the time spent in close interaction with stranger mice for each trial. The following parameters were considered: (1) social recognition, defined as the ability to identify a conspecific (Stranger 1 versus the empty cage) in Trial 2 (spending more time in the side-chamber containing Stranger 1); (2) social novelty, defined as the ability to discriminate between a novel mouse (Stranger 2) and a familiar mouse (Stranger 1) in Trial 5 (spending more time interacting with Stranger 2); and (3) sociability, which reflects the motivation of the test mouse to spontaneously interact with target mice in Trials 2-5.

### Social interaction in home cage (resident-intruder test)

We assessed social interaction in the home cage by standard protocols[52]. Briefly, we housed individual test mouse for 1 week before the task. Then, they were habituated for 30 min to the test room. In this task, a mouse in his home cage is allowed to freely roam in the absence of the cage top for 1 min. A novel juvenile (4-week-old) male intruder is then placed in the opposite corner as the resident subject and allowed to roam freely for 5 min. The task is recorded, and total physical interaction between the two mice is quantified visually; social interaction is scored as the time during which the resident mouse actively explores the intruder. We did not observe fighting, biting, or attacking in this task.

### Olfactory testing

After habituation to empty cages with no bedding, we tested mice for odor discrimination or sensitivity, as described[53]. In the discrimination task, mice are challenged with a filter paper embedded with an attractive scent (vanilla or cinnamon), an aversive scent (2-methyl butyrate), or a neutral scent (water). For the sensitivity task, dilutions of the same scent (vanilla) are used. The mice are videotaped, and the time spent sniffing the filter paper during a 3 min period is calculated *post hoc*.

### Novel object recognition task

We performed the object recognition task as described[54] following the no-habituation paradigm. The testing set-up was the same as for open field experiment. We placed mice in the testing room for at least 30 min for habituation. Then, mice were placed into the set-up containing two identical plastic sample objects (cube) placed 5 cm from one of the walls and ~12 cm apart. The mice were allowed to explore the environment for 10 min, during which we recorded their movements. After this familiarization session, we cleaned the objects and open-field with 70% ethanol to eliminate any olfactory cues, and returned the mice to their home cage for 2 min. We then placed the mice again in the open field, but this time a novel object of similar size and complexity (cylinder instead of a cube) replaced one of the objects present during the familiarization session. The mice were allowed to explore the environment for 10 min (test session), after which we returned them to their cages. For both sessions, we placed mice into the open field, with the head positioned opposite the objects. Object exploration, defined as the duration of time in which the head of the mouse faced less

than 2 cm from the object, was measured during the first 5 min of each session. We calculated the recognition index as the percentage of time spent exploring the novel object versus the total time spent exploring the objects.

## Drug injections

We diluted NBQX and AP5 (both from Tocris) in 0.9% saline solution and intraperitoneally injected them 10 min before the start of the test. Doses were 50 mg $kg^{-1}$ for NBQX and 10 mg $kg^{-1}$ for AP5. We injected at least 10 mice per genotype with each drug, but each mouse received only a single injection. We quantified the total interaction time with both Stranger 1 and Stranger 2 (Trial 5). To repress transgene expression, we fed mice with a diet containing doxycycline (200 mg $kg^{-1}$) (Bioserv). To ensure early repression, we maintained breeder mice on a doxycycline-containing diet. After weaning and genotyping, we fed mice with this diet until 8 months of age.

## Golgi staining

We processed mouse brains for morphological assessment with the FD Rapid Golgi Stain Kit (FD NeuroTechnologies) according to the manufacturer's protocol. We submerged mouse brains in impregnation solution for 14 d and then flash frozen in isopentane at −70 °C. Next, we cut 200 μm thick cryosections with a cryostat (Leica), mounted on gelatin-coated slides, rinsed in $dH_2O$, and incubated in developing solution for 10 min. Sections were dehydrated with increasing concentrations of ethanol, cleared with xylene, and coverslipped with Permount mounting medium.

We examined the slides with a Nikon inverted microscope at the imaging core facility (University of Massachusetts Medical School). We took image stacks of 40-120 μm segments of apical dendrites on pyramidal neurons of layer II-III of the mPFC or in the CA3 region with a 100X oil-immersion lens (N.A. 1.45). For spine analysis, we quantified 15-25 dendritic segments ($n$ = 3 mice per genotype). Total dendritic length was 1897 μm for *tTA:CHMP2B*$^{Intron5}$ mice and 1702 μm for *tTA:CHMP2B*$^{WT}$ mice. All image stacks were first deconvolved (with the iterative three-dimensional (3D) deconvolution plug-in for Image J) using a point-spread function (PSF) as a reference (PSF plug-in for ImageJ). We imported images into NeuronStudio for 3D analysis of spine density and spine size[4] and measured spines in 3D from the $z$-stacks. We calculated the density by dividing the total number of spines per 100 μm of dendrite. A spine was labeled thin if its head was < 0.6 μm in diameter and had a maximum length of at least twice the head diameter. We classified a spine as mushroom if its head diameter was > 0.6 μm. Stubby spines were those lacking a neck. We classified other spines as "other".

## AAV production and injections

We constructed AAV particles (serotype 9) as described[56]. As a control, we use an AAV-GFP vector so that no exogenous miRNA is expressed (limiting potentially off-target effects). We constructed AAV-GFP-miR-124 by inserting 500 bp of mouse pri-miR-124-1 into the 3′UTR of the GFP cassette of the control vector. Lentivirus expressing short hairpin RNA (shRNA) were from the University of Massachusetts RNAi core facility, which houses

the complete collection of mouse lentiviral shRNA libraries from Open Biosystems[57]. We packed lentivirus particles as described[58,59].

*tTA:CHMP2B$^{Intron5}$ and tTA:CHMP2B$^{WT}$* mice were deeply anesthetized with ketamine (100 mg kg$^{-1}$) and xylazine (10 mg kg$^{-1}$) and placed in a stereotaxic frame. The coordinates according to the mouse brain atlas of Paxinos & Franklin were: AP, 2.43 mm; ML, ± 0.28 mm; DV, −1.81mm relative to the bregma, angled 14° toward the midline in the coronal plane. We injected high-titer vector (0.8-1.2 × $10^{13}$; 1.5 μl) bilaterally. At the end of the behavioral experiments, we sectioned the brains of these mice to verify the accuracy and extent of transduction. We analyzed the data from mice with correct injections in the target area. To calculate transduction efficiency, we stained brains from mice infected with AAVs or lentivirus ($n$ = 6 per vector) with antibody against GFP before microscopic examination. For each mouse, we quantified the area transduced on four 20-μm-thick sections (bregma +2.2 to +1.9 mm) using Image J. The mean area of transduction per slice was 0.43 ± 0.095 mm$^2$ and 0.46 ± 0.087 mm$^2$ for AAVs and lentivirus, respectively.

## Electrophysiology

We conducted all experiments in accordance with the National Institutes of Health "Guidelines for the Care and Use of Laboratory Animals" and an approved animal protocol from the Harvard Medical Area Standing Committee on Animals.

We used *tTA:CHMP2B$^{WT}$* and *tTA:CHMP2B$^{Intron5}$* mice at 15-16 weeks of age. The brains were rapidly removed and placed in ice-cold artificial CSF (ACSF) containing 126 mM NaCl, 2.5 mM KCl, 2.5 mM $CaCl_2$, 1.2 mM $MgCl_2$, 25 mM $NaHCO_3$, 1.2 mM $NaH_2PO_4$, and 25 mM D-glucose. ACSF was saturated with 95% $O_2$ and 5% $CO_2$. We cut coronal cortical slices (300 μm) containing the mPFC with a Leica VT1200 Vibratome, and collected slices into a tissue incubator (Harvard Apparatus) and allowed them to recover for 1 h in a 32 °C water bath. We then incubated slices in oxygenated ACSF for 1 h at room temperature (21-23 °C) and transferred to a recording chamber continuously perfused with oxygenated ACSF.

We did whole-cell voltage-clamp recordings of individual layer V pyramidal neurons using an Axoclamp 2B or a Multiclamp 700B amplifier (Molecular Devices) under infrared differential interference contrast microscopy. We identified pyramidal neurons by their morphology and delivered presynaptic stimuli (0.033 Hz, 200 μs) with a concentric bipolar electrode (FHC) placed at layer II and III of the mPFC cortex. For recordings of evoked EPSCs and miniature EPSCs (mEPSCs), neurons were voltage clamped at −60 mV unless indicated otherwise. We recorded evoked EPSCs every 30 s. The superfusion medium contained picrotoxin (100 μM) to block $GABA_A$ receptor-mediated synaptic responses. We added tetrodotoxin (1 μM, Sigma) and AP5 (2-amino-5-phosphonopentanoic acid, 50 μM, Abcam Biochemicals) during recordings of mEPSCs. We filled recording pipettes with solution containing 142 mM Cs-gluconate, 8 mM NaCl, 10 mM HEPES, 0.4 mM EGTA, 2.5 mM QX-314 [*N*-(2,6-dimethylphenylcarbamoylmethyl)triethylammonium bromide], 2 mM Mg-ATP, and 0.25 mM GTP-Tris, pH 7.25. For all recordings, temperature was maintained at 32°C with a temperature controller (Warner Instruments). For the Naspm (1-naphthylacetyl spermine trihydrochloride) sensitivity assay, after stable EPSCs were

obtained for 10 min as baseline, we delivered the drug to the bath for 10-15 min with a gravity-driven perfusion system (Harvard Apparatus). We acquired data with a Digidata 1440A and pClamp software (version 10.2; Molecular Devices). Signals were filtered at 1 kHz, digitized at 10-20 kHz, and analyzed with Clampfit. We analyzed mEPSCs with Mini Analysis 6 (Synaptosoft).

### *In situ* hybridization and immunofluorescence

Mice were deeply anesthetized with ketamine (100 mg $kg^{-1}$) and xylazine (10 mg $kg^{-1}$) and perfused intracardially with ice-cold PBS and then with 4% paraformaldehyde. Brains were extracted, postfixed in the same fixative overnight at 4 °C, transferred to a 30% sucrose solution for cryoprotection, frozen, and stored at −80 °C. We sectioned brain samples with a standard cryostat.

We used standard protocols for *in situ* hybridization and immunofluorescence[60]. For detection of miR-124, we purchased digoxigenin-labeled LNA probes from Exiqon. For transgene expression, a biotin- or digoxigenin-labeled RNA probe was synthesized with gene-specific PCR primers (forward 5′-AAATAATACGACTCACTATAGGGAGATTCTTGATGA AATTGGAATTGAAAT-3′ and reverse 5′-GCAGTGAAAAAAATGCTTTATTTGT-3′) and cDNA templates from transgenic mouse brain. Probes were hybridized overnight at 55 °C, and the slides were incubated with horseradish peroxidase-conjugated antidigoxigenin antibody (Roche; 1:500) and steptavidin linked to the peroxidase (Roche). FITC or Cy3 TSA Plus kit (Perkin-Elmer) were used for final detection.

For immunofluorescence, we diluted primary antibodies in PBS containing 10% donkey serum (Sigma), 3% bovine albumin (Sigma), and 0.3% Triton X-100 and incubated overnight at 4 °C. Corresponding donkey anti-rabbit or anti-mouse Alexa 488 or 555 (Invitrogen) was used for secondary detection. The primary antibodies were anti-NeuN (Milipore, MAB377 1:1,000), PSD95 (NeuroMab, 75-028; 1:5,000), GFAP (Dako, Z0334; 1:2,000), Gria2 (Abcam, ab52932; 1:2,000), Gria4 (Abcam, ab77407; 1:1,000), ubiquitin (Enzo Life Sciences, BML-PW8810; 1;1000) and anti-GFP (Life Technologies, A11122; 1:3,000).

### Human brain samples

We obtained five FTD cases (3 men and 2 women, mean age at death 68 ± 6 years) and five age-matched normal controls (2 men and 3 women, mean age at death 79 ± 5 years) from the Mayo Clinic Jacksonville and the UCSF Neurodegenerative Disease Brain Bank. Informed consent was obtained for postmortem studies. Sex and postmortem interval (PMI) to autopsy were not different between cases and controls. FTD cases had sporadic behavioral variant FTD (bvFTD) due to FTLD-TDP, Type B. Control brains had no evidence of neurological disease either clinically or neuropathologically. We used frozen tissue (100-150 mg) from gray matter of the middle frontal gyrus for RNA extraction and subsequent RT-PCR analysis.

### Image acquisition and processing

For immunofluorescence and *in situ* hybridization, we acquired images with an Eclipse C1 confocal microscope and software (Nikon). We quantified the number of NeuN neurons from fluorescence images of four *tTA:CHMP2B*$^{WT}$ mice and four *tTA:CHMP2B*$^{Intron5}$ mice at 8 months of age; observers were blinded to genotype. For NeuN counting, we counted three to four sections of the mPFC with the Image J cell-counter plug-in.

For Gria puncta quantification, we used confocal z-stacks (159 × 159 × 10 μm). We analyzed three to four sections ($n$ = 3 mice per genotype) or two sections ($n$ = 6 mice per AAV vector). Following z-projection images, we quantified puncta using Particle Analyzer plug-in. We carried out GFAP coverage quantification as previously described[14].

### Northern blot

We extracted RNA from specific brain regions with Trizol reagent (Invitrogen) according to the manufacturer's instructions. We loaded 5–10 μg total RNA into a urea-containing 12.5% acrylamide gel (Sequagel-Ureagel, National Diagnostics) and electrophoresed in standard TBE (1x) buffer. We then transferred RNA to a positively charged nylon membrane (Amersham) and hybridized overnight with digoxigenin-labeled LNA probes (Exiqon). We used anti-digoxigenin antibody linked to alkaline phosphatase (Roche, 11 093 274 910; 1:10,000) and CDP-star reagent (Roche) for detection.

### Western blot

We obtained cortical extracts[61] and cortical PSD fractions[21] as described. PSD or cortical samples (20 μg) were subjected to SDS-PAGE and probed with specific primary antibodies. After incubation with the appropriate secondary antibody linked to horseradish peroxidase (Jackson Immunoresearch), West Pico Signal Chemoluminescent Substrate (Thermo) was used for detection. Antibodies used in these experiments included rabbit antibodies against CHMP2B (Abcam, ab 33174; 1:2,000), Gria1 (Abcam, ab109450; 1:5,000), Gria2 (Abcam, ab52932; 1:2,000), Gria3 (Abcam, ab78366; 1:1,000), Gria4 (Abcam, ab77407; 1:1,000), Grin1 (Upstate Biotechnology, 05-4320; 1:1,000), Grin2a (Upstate Biotechnology, 07-632; 1:2,000), Grin2b (Upstate Biotechnology, 0 -600; 1:1,000), p62 (Cell Signaling Technology, 5114; 1:2,000), and β-actin (Sigma, A-5316; 1:10,000) as a loading control.

### Luciferase assays

We cultured HEK cells in Dulbecco's modified Eagle's medium containing 10% fetal calf serum and split the day before transfection to achieve ~50% confluence at the time of transfection. We amplified 3′UTRs from *Gria1*, *Gria2*, *Gria3*, and *Gria4* transcripts by PCR from mouse brain cDNA and cloned downstream from the renilla luciferase coding sequence of the psicheck2 vector (Promega). We obtained 3′UTRs containing mutated miR-124 binding sites (WT binding site GUGCCUA; mutated binding site GUCGAAAA) by PCR with specific primers including the mutated nucleotide sequence. We transfected cells with a plasmid containing an AMPAR subunit 3′UTR together with a vector driving the expression of miR-124 or miR-9 or an empty vector (pSuper, Oligoengine). For transfection, we used Fugene (Roche) according to the manufacturer's instructions. After 24

h, we lysed the cells and measured luciferase activity with the Dual Luciferase Reporter Assay (Promega), and normalized results to firefly luciferase activity.

## Quantitative RT-PCR

We extracted RNA with the miRNeasy kit (Qiagen) according to the manufacturer's instructions and digested with DNase for 30 min on-column. We performed first-strand synthesis with 500 ng of total RNA, random hexamers, and TaqMan reverse transcription reagents (Applied Biosystems). Reactions without reverse transcription were always included.

For quantitative PCR, we designed and tested specific primers (Supplementary Table 2) at different cDNA dilutions, and calculated their efficiency. We only used primers showing 95–105% efficiency for further analysis. We performed real-time quantitative PCR with a StepOnePlus system (Applied Biosystems). We carried out reactions (in triplicate) with SYBR Green PCR Master Mix (Applied Biosystems). Each SYBR Green reaction (total volume, 20 μl) contained 1 μl of cDNA as template and each primer at 0.25 μM. Controls without template DNA (reverse transcription minus reaction) were always negative. We incubated he reactions at 95 °C for 10 min to activate the HotStar *Taq* polymerase followed by 40 cycles at 95 °C for 15 s (denaturation) and at 60 °C for 1 min (annealing and extension). We used β-Actin or GADPH as internal control. Because SYBR Green indiscriminately binds to double-stranded DNA, other products in the PCR such as primer dimers may be detected along with the target gene. To verify that the SYBR Green dye detected only one PCR product, we subjected the samples to the heat dissociation protocol after the final cycle of PCR to check for the presence of only one peak.

Given the limited amount of human samples available, we used TaqMan miRNAs assays to quantify miRNA abundance in brain tissues and iPS-derived neurons (Applied Biosystems, assay 001182 for miR-124 and assay 000583 for miR-9). We extracted RNA as described for mouse samples. Then, we used specific primers for each miRNA for both reverse transcription and subsequent TaqMan quantitative PCR as specified by the manufacturer. We used U6 as internal reference gene for those experiments.

## Mouse cortical cultures and iPSC-derived neuronal cultures

To test the efficiency of *Gria2* shRNAs, we prepared neuronal cortical cultures from newborn mice as described[10]. 2 d after plating, 250 μl of lentiviral supernatant was added to the medium. We allowed cells to grow for 3 d and then lysed cells for protein extraction, and assessed Gria2 levels by western blot.

For iPSC-derived neuronal cultures, we used four different lines from three subjects with bvFTD. Two of these lines carry the progranulin S116X mutation[36]; the other two lines were derived from two subjects with bvFTD caused by C9ORF72 repeat expansion[37]. We used two iPSC lines from one healthy subject[36] as controls and performed neuronal differentiation as described[36,37].

### Statistical analysis

We performed all statistical analyses with Prism GraphPad 6.0. We compared *tTA:CHMP2B*$^{WT}$ and *tTA:CHMP2B*$^{Intron5}$ mice for each behavioral task. We used the Student's *t* test to detect genotype differences in electrophysiological experiments, qPCR, NeuN counting, biochemical analysis, and some behavioral tests. For shRNA efficiency, we used one-way ANOVA. We also used repeated-measure two-way ANOVA to detect differences in the AAV injections. We used Bonferroni's or Fisher's LSD test after ANOVA results and analyzed the results of antagonist injections with the Kruskal-Wallis test corrected for multiple comparisons. We used Mann-Whitney test for comparisons of brain human samples.

## Supplementary Material

Refer to Web version on PubMed Central for supplementary material.

## ACKNOWLEDGMENTS

We thank S. Ordway and Gao lab members for comments, Y. Li and A. Philbrook for help with some experiments, Andrew Tapper for sharing behavioral test equipment, the Digital Light Microscopy Core at the University of Massachusetts Medical School (UMMS) for assistance with Golgi staining, the UMMS Viral Vector core for help with AAV vectors, and University of California San Francisco (UCSF) Neurodegenerative Disease Brain Bank for some human brain tissues. We also thank R. Rademakers for genotyping some human samples in a previous work[51] that we used in the current study, and A. Chen-Plotkin for sharing published array data[38,40]. This work was supported by a UMMS startup fund (F.-B.G.), The Consortium for Frontotemporal Dementia Research (W.W.S.), and the US National Institutes of Health (NS057553, NS066586 and NS079725 to F.-B.G., DA032283 to W.D.Y., MH086509 to S.A., AG023501, AG19724 to W.W.S., AG016574 to D.W.D. and L.P.

## REFERENCES

1. Dickson DW. Parkinson's disease and parkinsonism: neuropathology. Cold Spring Harb. Perspect. Med. 2012; 2:a009258. [PubMed: 22908195]
2. Goldstein LH, Abrahams S. Changes in cognition and behaviour in amyotrophic lateral sclerosis: nature of impairment and implications for assessment. Lancet Neurol. 2013; 12:368–380. [PubMed: 23518330]
3. Serrano-Pozo A, Frosch MP, Masliah E, Hyman BT. Neuropathological alterations in Alzheimer disease. Cold Spring Harb. Perspect. Med. 2011; 1:a006189. [PubMed: 22229116]
4. Neary D, Snowden J, Mann D. Frontotemporal dementia. Lancet Neurol. 2005; 4:771–780. [PubMed: 16239184]
5. Loy CT, Schofield PR, Turner AM, Kwok JB. Genetics of dementia. Lancet. 2014; 383:828–840. [PubMed: 23927914]
6. Gendron TF, Belzil VV, Zhang YJ, Petrucelli L. Mechanisms of toxicity in C9FTLD/ALS. Acta Neuropathol. 2014; 127:359–376. [PubMed: 24394885]
7. Ling SC, Polymenidou M, Cleveland DW. Converging mechanisms in ALS and FTD: disrupted RNA and protein homeostasis. Neuron. 2013; 79:416–438. [PubMed: 23931993]
8. Cox LE, et al. Mutations in CHMP2B in lower motor neuron predominant amyotrophic lateral sclerosis (ALS). PLoS One. 2010; 5:e9872. [PubMed: 20352044]
9. Skibinski G, et al. Mutations in the endosomal ESCRTIII-complex subunit CHMP2B in frontotemporal dementia. Nat. Genet. 2005; 37:806–808. [PubMed: 16041373]
10. Hooli BV, et al. Rare autosomal copy number variations in early-onset familial Alzheimer's disease. Mol. Psychiatry. 2013; 19:676–681. [PubMed: 23752245]
11. Henne WM, Buchkovich NJ, Emr SD. The ESCRT pathway. Dev. Cell. 2011; 21:77–91. [PubMed: 21763610]

12. Hurley JH, Hanson PI. Membrane budding and scission by the ESCRT machinery: it's all in the neck. Nat. Rev. Mol. Cell. Biol. 2010; 11:556–566. [PubMed: 20588296]
13. Belly A, et al. CHMP2B mutants linked to frontotemporal dementia impair maturation of dendritic spines. J. Cell Sci. 2010; 123:2943–2954. [PubMed: 20699355]
14. Ghazi-Noori S, et al. Progressive neuronal inclusion formation and axonal degeneration in CHMP2B mutant transgenic mice. Brain. 2012; 135:819–832. [PubMed: 22366797]
15. Lee JA, Beigneux A, Ahmad ST, Young SG, Gao FB. ESCRT-III dysfunction causes autophagosome accumulation and neurodegeneration. Curr. Biol. 2007; 17:1561–1567. [PubMed: 17683935]
16. Lee JA, Gao FB. Inhibition of autophagy induction delays neuronal cell loss caused by dysfunctional ESCRT-III in frontotemporal dementia. J. Neurosci. 2009; 29:8506–8511. [PubMed: 19571141]
17. Abe M, Bonini NM. MicroRNAs and neurodegeneration: role and impact. Trends Cell Biol. 2013; 23:30–36. [PubMed: 23026030]
18. Gascon E, Gao FB. Cause or effect: Misregulation of microRNA pathways in neurodegeneration. Front. Neurosci. 2012; 6:48. [PubMed: 22509148]
19. Gao FB. Context-dependent functions of specific microRNAs in neuronal development. Neural Dev. 2010; 5:25. [PubMed: 20920300]
20. Yizhar O, et al. Neocortical excitation/inhibition balance in information processing and social dysfunction. Nature. 2011; 477:171–178. [PubMed: 21796121]
21. Peca J, et al. Shank3 mutant mice display autistic-like behaviours and striatal dysfunction. Nature. 2011; 472:437–442. [PubMed: 21423165]
22. Rademakers R, Neumann M, Mackenzie IR. Advances in understanding the molecular basis of frontotemporal dementia. Nat. Rev. Neurol. 2012; 8:423–434. [PubMed: 22732773]
23. Seelaar H, Rohrer JD, Pijnenburg YA, Fox NC, van Swieten JC. Clinical, genetic and pathological heterogeneity of frontotemporal dementia: a review. J. Neurol. Neurosurg. Psychiatry. 2011; 82:476–486. [PubMed: 20971753]
24. Bourne J, Harris KM. Do thin spines learn to be mushroom spines that remember? Curr. Opin. Neurobiol. 2007; 17:381–386. [PubMed: 17498943]
25. Kasai H, Matsuzaki M, Noguchi J, Yasumatsu N, Nakahara H. Structure-stability-function relationships of dendritic spines. Trends Neurosci. 2003; 26:360–368. [PubMed: 12850432]
26. Kasai H, Fukuda M, Watanabe S, Hayashi-Takagi A, Noguchi J. Structural dynamics of dendritic spines in memory and cognition. Trends Neurosci. 2010; 33:121–129. [PubMed: 20138375]
27. Namba T, Morimoto K, Sato K, Yamada N, Kuroda S. Antiepileptogenic and anticonvulsant effects of NBQX, a selective AMPA receptor antagonist, in the rat kindling model of epilepsy. Brain Res. 1994; 638:36–44. [PubMed: 8199874]
28. Lu W, et al. Subunit composition of synaptic AMPA receptors revealed by a single-cell genetic approach. Neuron. 2009; 62:254–268. [PubMed: 19409270]
29. Rozov A, Sprengel R, Seeburg PH. GluA2-lacking AMPA receptors in hippocampal CA1 cell synapses: evidence from gene-targeted mice. Front. Mol. Neurosci. 2012; 5:22. [PubMed: 22375105]
30. Cull-Candy S, Kelly L, Farrant M. Regulation of Ca2+-permeable AMPA receptors: synaptic plasticity and beyond. Curr. Opin. Neurobiol. 2006; 16:288–297. [PubMed: 16713244]
31. Liu SJ, Zukin RS. Ca2+-permeable AMPA receptors in synaptic plasticity and neuronal death. Trends Neurosci. 2007; 30:126–134. [PubMed: 17275103]
32. Noh KM, et al. Blockade of calcium-permeable AMPA receptors protects hippocampal neurons against global ischemia-induced death. Proc. Natl. Acad. Sci. U. S. A. 2005; 102:12230–12235. [PubMed: 16093311]
33. Ambros V. The functions of animal microRNAs. Nature. 2004; 431:350–355. [PubMed: 15372042]
34. Siegel G, Saba R, Schratt G. microRNAs in neurons: manifold regulatory roles at the synapse. Curr. Opin. Genet. Dev. 2011; 21:491–497. [PubMed: 21561760]

35. Deo M, Yu JY, Chung KH, Tippens M, Turner DL. Detection of mammalian microRNA expression by in situ hybridization with RNA oligonucleotides. Dev. Dyn. 2006; 235:2538–2548. [PubMed: 16736490]
36. Almeida S, et al. Induced pluripotent stem cell models of progranulin-deficient frontotemporal dementia uncover specific reversible neuronal defects. Cell Rep. 2012; 2:789–798. [PubMed: 23063362]
37. Almeida, et al. Modeling key pathological features of frontotemporal dementia with C9ORF72 repeat expansion in iPSC-derived human neurons. Acta Neuropathol. 47:115–123.
38. Chen-Plotkin AS, et al. TMEM106B, the risk gene for frontotemporal dementia, is regulated by the microRNA-132/212 cluster and affects progranulin pathways. J. Neurosci. 2012; 32:11213–11227. [PubMed: 22895706]
39. Hebert SS, Wang WX, Zhu Q, Nelson PT. A study of small RNAs from cerebral neocortex of pathology-verified Alzheimer's disease, dementia with Lewy bodies, hippocampal sclerosis, frontotemporal lobar dementia, and non-demented human controls. J. Alzheimers. Dis. 2013; 35:335–348. [PubMed: 23403535]
40. Chen-Plotkin AS, et al. Variations in the progranulin gene affect global gene expression in frontotemporal lobar degeneration. Hum. Mol. Genet. 2008; 17:1349–1362. [PubMed: 18223198]
41. van Swieten JC, Heutink P. Mutations in progranulin (GRN) within the spectrum of clinical and pathological phenotypes of frontotemporal dementia. Lancet Neurol. 2008; 7:965–974. [PubMed: 18771956]
42. Wang F, et al. Bidirectional control of social hierarchy by synaptic efficacy in medial prefrontal cortex. Science. 2011; 334:693–697. [PubMed: 21960531]
43. Piguet O, Hornberger M, Mioshi E, Hodges JR. Behavioural-variant frontotemporal dementia: diagnosis, clinical staging, and management. Lancet Neurol. 2011; 10:162–172. [PubMed: 21147039]
44. Filiano AJ, et al. Dissociation of frontotemporal dementia-related deficits and neuroinflammation in progranulin haploinsufficient mice. J. Neurosci. 2013; 33:5352–5361. [PubMed: 23516300]
45. Kim EJ, et al. Selective frontoinsular von Economo neuron and fork cell loss in early behavioral variant frontotemporal dementia. Cereb. Cortex. 2012; 22:251–259. [PubMed: 21653702]
46. Adamczyk A, et al. GluA3-deficiency in mice is associated with increased social and aggressive behavior and elevated dopamine in striatum. Behav. Brain Res. 2012; 229:265–272. [PubMed: 22285418]
47. Bezprozvanny I, Hiesinger PR. The synaptic maintenance problem: membrane recycling, Ca2+ homeostasis and late onset degeneration. Mol. Neurodegener. 2013; 8:23. [PubMed: 23829673]
48. Gibbings DJ, Ciaudo C, Erhardt M, Voinnet O. Multivesicular bodies associate with components of miRNA effector complexes and modulate miRNA activity. Nat. Cell Biol. 2009; 11:1143–1149. [PubMed: 19684575]
49. Lee YS, et al. Silencing by small RNAs is linked to endosomal trafficking. Nat. Cell Biol. 2009; 11:1150–1156. [PubMed: 19684574]
50. Dutta R, et al. Hippocampal demyelination and memory dysfunction are associated with increased levels of the neuronal microRNA miR-124 and reduced AMPA receptors. Ann. Neurol. 2013; 73:637–645. [PubMed: 23595422]
51. Prudencio M, et al. Misregulation of human sortilin splicing leads to the generation of a nonfunctional progranulin receptor. Proc. Natl. Acad. Sci. U. S. A. 2012; 109:2151–21515.
52. Winslow JT. Mouse social recognition and preference. Curr. Protoc. Neurosci. 2003; 22:8.16.1–8.16.16.
53. Witt RM, Galligan MM, Despinoy JR, Segal R. Olfactory behavioral testing in the adult mouse. J. Vis. Exp. 2009; 23:949. [PubMed: 19229182]
54. Leger M, et al. Object recognition test in mice. Nat. Protoc. 2013; 8:2531–2537. [PubMed: 24263092]
55. Rodriguez A, Ehlenberger DB, Dickstein DL, Hof PR, Wearne SL. Automated three-dimensional detection and shape classification of dendritic spines from fluorescence microscopy images. PLoS One. 2008; 3:e1997. [PubMed: 18431482]

56. Mueller C, Ratner D, Zhong L, Esteves-Sena M, Gao G. Production and discovery of novel recombinant adeno-associated viral vectors. Curr Protoc Microbiol. 2012; 26:14D.1.1–14D.1.21.

57. Chang K, Elledge SJ, Hannon GJ. Lessons from Nature: microRNA-based shRNA libraries. Nat. Methods. 2006; 3:707–714. [PubMed: 16929316]

58. Gao, GP.; Sena-Esteves, M. Introducing Genes into Mammalian Cells: Viral Vectors. In: Green, MR.; Sambrook, J., editors. Molecular Cloning, Vol 2: A Laboratory Manual. Cold Spring Harbor Laboratory Press; New York: 2012. p. 1209-1313.

59. Kutner RH, Zhang XY, Reiser J. Production, concentration and titration of pseudotyped HIV-1-based lentiviral vectors. Nat. Protoc. 2009; 4:495–505. [PubMed: 19300443]

60. Gascon E, et al. Hepatocyte growth factor-Met signaling is required for Runx1 extinction and peptidergic differentiation in primary nociceptive neurons. J. Neurosci. 2010; 30:12414–12423. [PubMed: 20844136]

61. Gascon E, Vutskits L, Jenny B, Durbec P, Kiss JZ. PSA-NCAM in postnatally generated immature neurons of the olfactory bulb: a crucial role in regulating p75 expression and cell survival. Development. 2007; 134:1181–1190. [PubMed: 17301083]

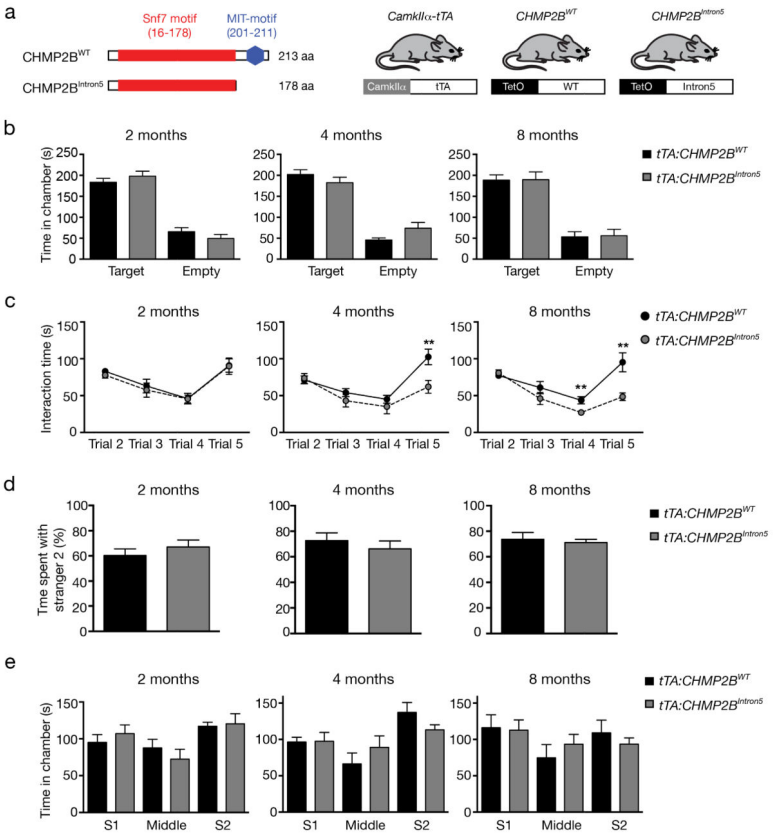


**Figure 1.**

Age-dependent deficits in sociability in *tTA:CHMP2B*$^{Intron5}$ mice. (**a**) Schematic representation of the wildtype and mutant CHMP2B proteins and the transgenic mouse strains used. (**b**) Social recognition, namely total time spent in the target chamber and empty chamber in Trial 2 at different ages, is measured in *tTA:CHMP2B*$^{Intron5}$ mice ($n$ = 11 mice per genotype, p > 0.6 by two-sided $t$ test). (**c**) Sociability of *tTA:CHMP2B*$^{WT}$ and *tTA:CHMP2B*$^{Intron5}$ mice are measured based on interaction time ($n$ = 11 mice per genotype. **: $P < 0.01$ by two-sided $t$ test). (**d**) Proportion of interaction time spent with Stranger 2 in Trial 5 was measured as an indicator for social memory and novelty in *tTA:CHMP2B*$^{WT}$ and *tTA:CHMP2B*$^{Intron5}$ mice ($n$ = 11 mice per genotype; $P > 0.5$ by two-sided $t$ test). All values are mean ± s.e.m. (**e**) Time spent in each chamber during Trial 5 was quantified as the exploration patterns ($n$ = 11 mice per genotype; $P > 0.5$ by two-sided $t$ test). All values are mean ± s.e.m.

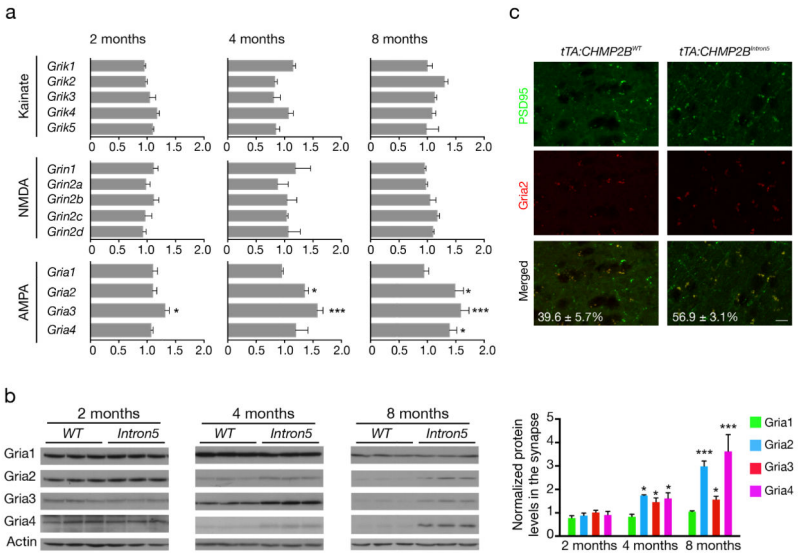


**Figure 2.**

Biochemical characterization of glutamate receptor subunits in the cortex of *tTA:CHMP2B*$^{Intron5}$ mice. (**a**) Quantitative RT-PCR analysis of mRNA levels of different glutamate receptor subunits (kainate, NMDA, and AMPA) in *tTA:CHMP2B*$^{Intron5}$ and *tTA:CHMP2B*$^{WT}$ mice ($n$ = 3 mice per genotype; *: $P < 0.05$, ***: $P < 0.001$ by two-sided $t$ test). (**b**) Western blot analysis of the expression levels of AMPAR subunits in the PSD fractions of *tTA:CHMP2B*$^{WT}$ and *tTA:CHMP2B*$^{Intron5}$ mice of different ages ($n$ = 3 mice per genotype, *: $P < 0.05$, ***: $P < 0.001$ by two-sided $t$ test). (**c**) Double-immunostaining analysis and quantification of PSD95-positive (green) and Gria2-positive (red) puncta in the mPFC (layers II and III) of 8-month-old mice ($n$ = 3 mice per genotype, $P < 0.02$ by two-sided $t$ test). Scale bar, 200 μm. All values are mean ± s.e.m.

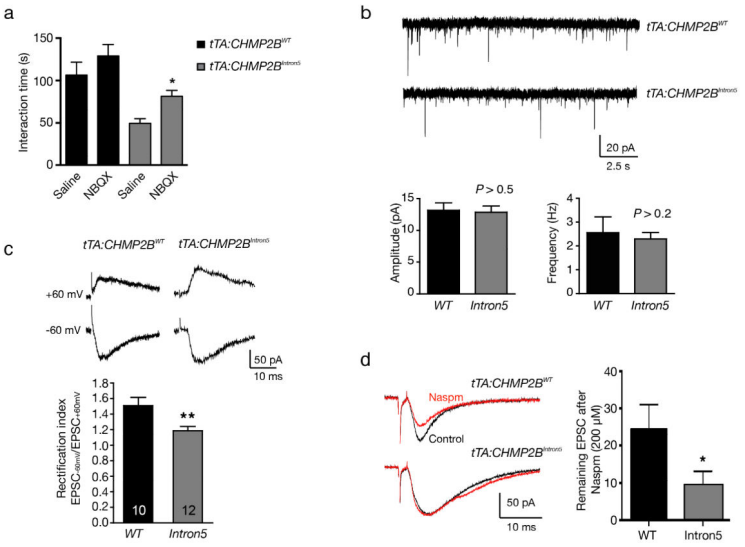


**Figure 3.**

Functional consequences of altered AMPAR composition in *tTA:CHMP2B*$^{Intron5}$ mice. (**a**) Behavioral consequences of AMPAR inhibitor NBQX in *tTA:CHMP2B*$^{WT}$ and *tTA:CHMP2B*$^{Intron5}$ mice at 8 months of age ($n$ = 10 for all groups except $n$ = 13 for *tTA:CHMP2B*$^{WT}$ saline; *: $P < 0.05$ by two-sided Kruskal-Wallis test corrected for multiple comparisons). (**b**) Whole-cell patch-clamp recordings of mEPSCs in pyramidal neurons in the mPFC. The amplitude and frequency of these miniature events were compared between *tTA:CHMP2B*$^{WT}$ mice ($n$ = 11) and *tTA:CHMP2B*$^{Intron5}$ mice ($n$ = 12, $P > 0.1$ by two-sided $t$ test). (**c**) The rectification index, calculated as $EPSC_{-60}/EPSC_{+60}$, for AMPAR-mediated EPSCs, was measured ($n$ = 10 for *tTA:CHMP2B*$^{WT}$ mice and $n$ = 12 for *tTA:CHMP2B*$^{Intron5}$ mice; **: $P < 0.01$ by two-sided $t$ test). (**d**) Decreased sensitivity of evoked EPSCs to Naspm (200 µM) inhibition in pyramidal neurons expressing $CHMP2B^{Intron5}$. Representative EPSC traces at −60 mV before (Control) and after Naspm application are shown on the left ($n$ = 8 mice for *tTA:CHMP2B*$^{WT}$ and $n$ = 9 for *tTA:CHMP2B*$^{Intron5}$. *: $P <$ 0.05 by two-sided $t$ test). Mice used in **b**-**d** were 15-16 weeks of age. All values are mean ± s.e.m.

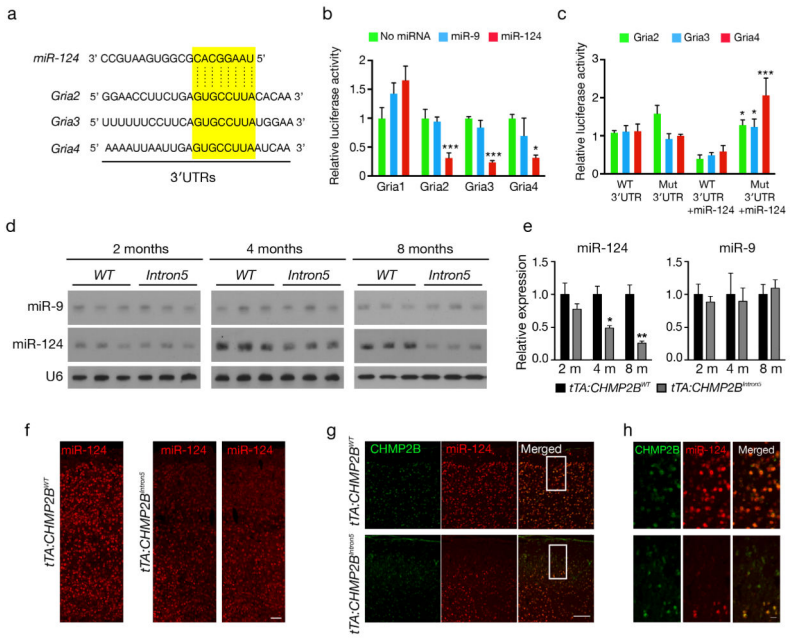


**Figure 4.**

MiR-124 targets AMPAR subunits, and its expression is reduced in the cortex of *tTA:CHMP2B*$^{Intron5}$ mice. (**a**) Alignment of potential binding sites for miR-124 in the 3′UTRs of *Gria2*, *Gria3*, and *Gria4* mRNAs. (**b**) Direct interaction between 3′UTRs of *Gria2*, *Gria3*, and *Gria4* mRNAs and miR-124 ($n > 4$ assays, *: $P < 0.05$, ***: $P < 0.001$ by two-sided *t* test). (**c**) The effects of miR-124 on the expression of luciferase-containing subunit 3′UTRs in which we mutated the miR-124 binding site. $n = 4$ assays, *: $P < 0.05$, **: $P < 0.001$ by two-sided *t* test. (**d**) Northern blot analysis of miR-9 and miR-124 expression levels in the cortex of *tTA:CHMP2B*$^{WT}$ and *tTA:CHMP2B*$^{Intron5}$ mice at different ages. (**e**) Quantification of the northern blots in panel d ($n = 3$ mice per group; *: $P < 0.05$, **: $P < 0.01$ by two-sided *t* test). (**f**) Fluorescence *in situ* hybridization of miR-124 in brain sections of *tTA:CHMP2B*$^{WT}$ and *tTA:CHMP2B*$^{Intron5}$ mice at 8 months of age. (**g**) Double-fluorescence *in situ* hybridization staining of miR-124 (red) in CHMP2B$^{Intron5}$-expressing cells (green) in the cortex at 8 months of age. Scale bar, 150 μm in f and g. (**h**) Higher magnification of the boxed area in G. Scar bar, 20 μm. Values are mean ± s.e.m. in **b** and **c** and mean ± s.d. in **e**.

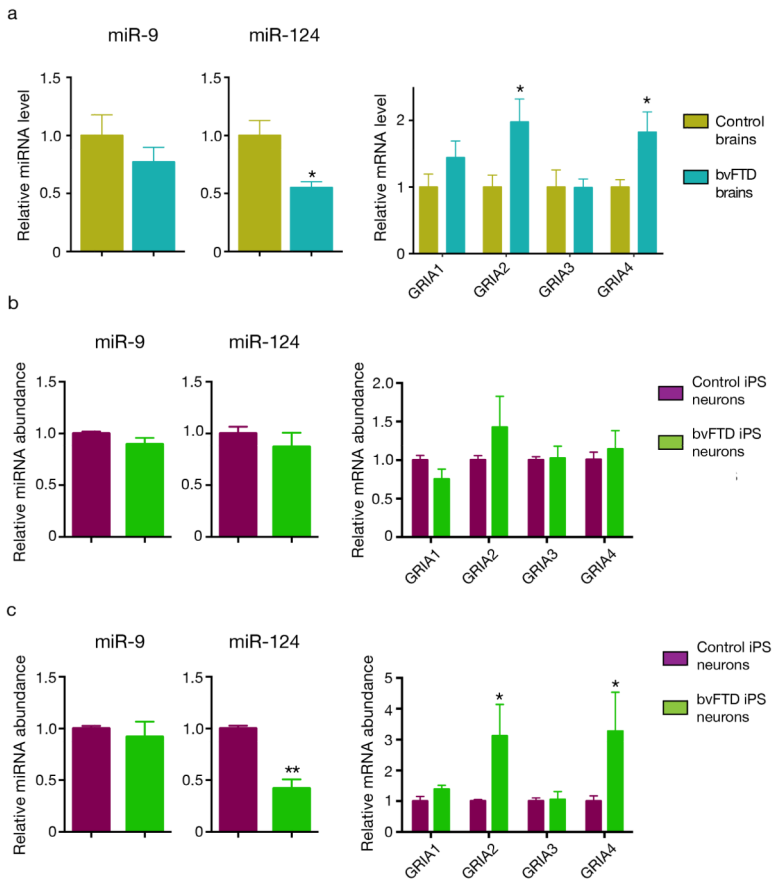


**Figure 5.**

miR-124 and AMPAR levels are altered in the frontal cortex of subjects with bvFTD and in cortical neurons derived from iPSC lines of three subjects with bvFTD. (**a**) Quantification of the abundance of miR-124, miR-9, and AMPAR transcripts by RT-PCR in the frontal cortex of subjects with bvFTD and controls. We normalized the content of AMPAR mRNAs against the geometric mean of four different neuronal-specific reference genes (MAP2, Enolase 2, GAP43, and PSD95). *: $P < 0.05$ by Mann-Whitney test. (**b**) Quantification of miR-124, miR-9, and AMPAR transcripts in 2-week old human neurons derived from 3 iPSC lines of two control individuals and 4 iPSC lines from three subjects with bvFTD[36,37]. $P > 0.1$ by two-sided *t* test). (**c**) The levels of miR-124, miR-9, and AMPAR transcripts were measured again in these human neurons at 8 weeks (*: $P < 0.05$, **: $P < 0.01$, ***: $P < 0.001$ by two-sided *t* test). All values are mean ± s.e.m.

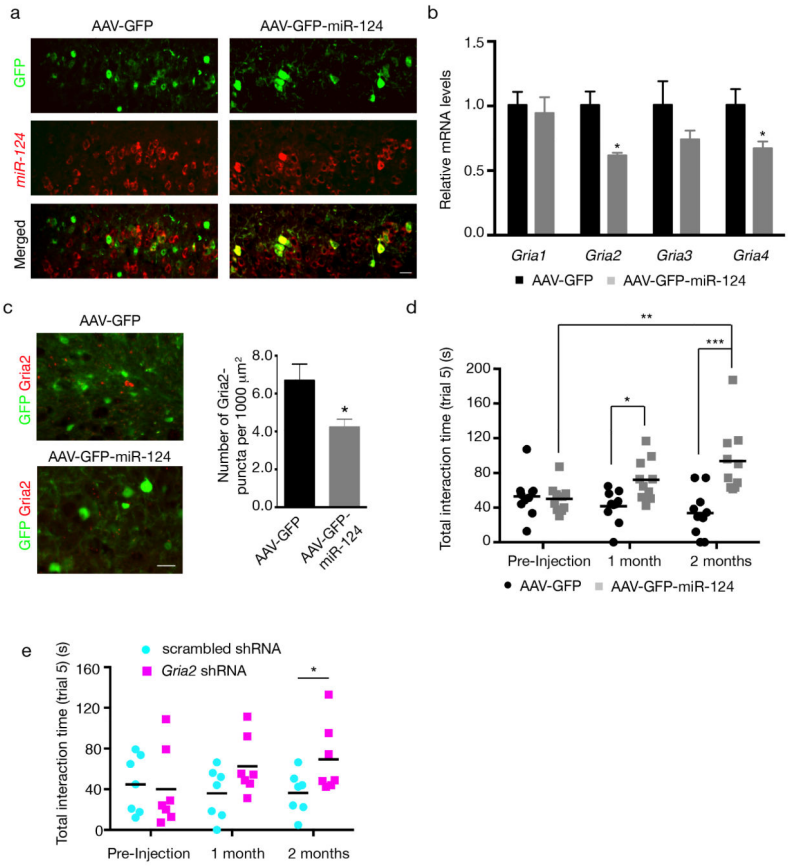


**Figure 6.**

miR-124 expression and Gria2 knockdown in the mPFC partially rescue social deficits in *tTA:CHMP2B*$^{Intron5}$ mice. (**a**) Double staining for GFP and miR-124 in *tTA:CHMP2B*$^{Intron5}$ mice (8 months) that received an intracranial injection of AAV-GFP (left panels) or AAV-GFP-miR-124 (right panels). To facilitate assessment of differences in miR-124 levels, we took pictures at the periphery of the injection site so infected and noninfected cells are present in the same field. miR-124 levels were similar in AAV-GFP-infected cells and noninfected neighboring cells. In contrast, AAV-GFP-miR-124 induced a robust increase in miR-124 expression. (**b**) qRT-PCR analysis of Gria transcripts in the mPFC of *tTA:CHMP2B*$^{Intron5}$ mice 2 months after AAV injection ($n$ = 5 AAV-GFP-infected mice and $n$ = 4 AAV-GFP-miR-124-infected mice; *: $P < 0.05$ by two-sided $t$ test). (**c**) Quantification of the number of Gria2-positive puncta in *tTA:CHMP2B*$^{Intron5}$ mice 2 months after intracranial injection of AAV-GFP or AAV-GFP-miR-124 ($n$ = 3 mice per genotype, *: $P < 0.05$ by two-sided $t$ test). (**d**) Quantification of miR-124-dependent rescue of social deficits in *tTA:CHMP2B*$^{Intron5}$ mice 1 and 2 months after bilateral injection. Sociability was significantly greater in mice injected with AAV-GFP-miR-124 in than in those injected with the control vector ($n$ = 10 per AAV vector; *: $P < 0.05$, **: $P < 0.01$, ***: $P < 0.001$ by two-sided repeated-measures two-way ANOVA corrected for multiple comparison, Bonferroni test). (**e**) Quantification of the rescue effects of *in vivo* downregulation of *Gria2* expression on social deficits in *tTA:CHMP2B*$^{Intron5}$ mice ($n$ = 7 per group; *: $P < 0.05$, by two-sided

repeated-measures two-way ANOVA followed by Fisher's LSD test). Scar bar, 20 μm. All values are mean ± s.e.m.